UNIVERSIDADE DE SÃO PAULO

INSTITUTO DE FÍSICA
CAIXA POSTAL 20516
01000 - SÃO PAULO - SP
BRASIL

publicações

IFUSP/P-420

THE ^{144}Sm(p,p') SCATTERING THROUGH ISOBARIC ANALOG RESONANCES AND THE STRUCTURE OF ^{145}Sm

M.L. Cescato and M.C.H.M. Ruiz
Instituto de Física, Universidade de São Paulo

J.L. Foster Jr.
Dept. of Physics, University of Notre Dame,
Notre Dame, Indiana 46556 and
Intermetrics, Inc., Warminster, PA 19044

and

F. Krmpotić
Instituto de Física Universidade de São Paulo
and
Departamento de Física, Facultad de Ciencias
Exactas, Universidad Nacional de La Plata,
1900 La Plata, Argentina

Julho/1983

THE ^{144}Sm(p,p') SCATTERING THROUGH ISOBARIC ANALOG RESONANCES AND THE STRUCTURE OF ^{145}Sm

M.L. CESCATO and M.C.H.M. RUIZ
Instituto de Física, Universidade de São Paulo
São Paulo, Brasil

J.L. FOSTER JR.
Dept. of Physics, University of Notre Dame
Notre Dame, Indiana 46556 and
Intermetrics, Inc., Warminster, PA 19044
and

F. KRMPOTIĆ*
Instituto de Física, Universidade de São Paulo
São Paulo, Brasil

and

Departamento de Física, Facultad de Ciencias Exactas,
Universidad Nacional de La Plata, 1900 La Plata, Argentina

Angular distributions of the cross section for the elastic and inelastic scattering of protons have been measured at four isobaric analog resonances of the ^{144}Sm + p system and at two off-resonance energies. Spectroscopic information about the $7/2_1^-$, $3/2_1^-$, $1/2_1^-$ and $5/2_1^-$ states of the parent nucleus ^{145}Sm is extracted, with the core ^{144}Sm in the states 0_1^+, 2_1^+, 3_1^-, 4_1^+ and 2_2^+. The analysis includes direct and fluctuating non-resonant processes. The direct scattering amplitude is obtained from a coupled channel treatment. Different methods for the calculations of the single-particle widths have been employed. The experimental spectroscopic amplitudes were confronted with nuclear structure calculations based on the particle-vibrator model. Both the liquid drop model and the quasi-particle random phase approximation were used to describe the vibrator. The calculations based on the later model show good agreement with the experimental results.

NUCLEAR REACTIONS ^{144}Sm(p,p'), E=8.5-14 MeV, enriched targets, measured $\sigma(E_p,\theta)$; experimental and theoretical ^{145}Sm spectroscopic amplitudes.

* Permanent address: Departamento de Física, Facultad de Ciencias Exactas, Universidad Nacional de La Plata, 1900 La Plata, Argentina. Fellow of the Consejo Nacional de Investigaciones Científicas y Técnicas de Argentina.

I. INTRODUCTION

Several experimental studies of the isobaric analog resonances in the ^{144}Sm + p system (^{145}Eu) have been reported[1-4] so far. In these works information about energies, widths, spins and parities of the resonances, associated with the low-lying states of the parent nucleus ^{145}Sm, were obtained through the analysis of elastic excitation functions. A few works appear in the literature on inelastic decays, namely, several highly excited particle-hole states in ^{144}Sm were studied by Martin et al.[3] while the decay to the first excited 2^+ state was analysed by Clement et al.[4] employing the DWBA prescription to account for the non-resonant scattering.

In the present work we analyse the elastic and inelastic decays of the isobaric analog resonances in ^{144}Sm+p system associated with four low-lying states of the parent nucleus ^{145}Sm. We consider the inelastic decays to the 2_1^+, 3_1^-, 4_1^+ and 2_2^+ states of ^{144}Sm, as the experimental data reported by Martin et al.[3] clearly indicates that all of then play an important role in building up the wave functions of the considered parent nucleus states. We make use of the coupled channel formalism for treating the direct non-resonant scattering. In addition, we also include the fluctuating non-resonant contributions to the cross-section (Hauser-Feshbach). This effect is usually ignored since the fluctuating decay occurs preferentially through the open neutron channel, turning negligible the fluctuating contribution in the proton channel. This, however, is not the case for the first two

isobaric resonances in the ^{144}Sm + p system, since they lie near the neutron threshold.

The determination of spectroscopic amplitudes involves theoretical estimates for single-particle resonance amplitudes (g^{sp}) and it was established by Harney and Weidenmüller[5] that the results may vary appreciably depending on the approach employed in treating the absorption in the $T_<$-states. In the present work we calculated the single particle resonance amplitudes using four different approaches[6-10]. The application of sum rules to the spectroscopic amplitudes resulting from the various approaches for g^{sp} provides us a check on the reliability of the various methods, along with a test of consistency for the experimental spectroscopic amplitudes.

Theoretical predictions for the spectroscopic amplitudes are obtained in the framework of the particle-vibrator model and compared to the experimental values. The vibrator is described at first by a liquid drop and later on treated within the quasi-particle random phase approximation (QRPA).

II. EXPERIMENT

The experiment was performed at the Universidade de São Paulo, Pelletron-8UD accelerator laboratory. Angular distributions of the elastic and inelastic cross sections of protons scattered by ^{144}Sm were measured at the beam energies 9.315, 10.205, 10.905 and 10.985 MeV. These values are equal or very close to the energies of the first $7/2^-$, $3/2^-$, $1/2^-$ and $5/2^-$

analog resonances in the ^{144}Sm + p system. The $7/2^-$ resonance was located by looking for the maximum yield of the protons leaving ^{144}Sm in the neutron particle-hole states[3]. The angular distributions were measured in 10° steps from $\theta_{Lab} = 40^\circ$ to 169°. In order to obtain informations about the non-resonant background additional angular distributions were observed at 8.50 and 14.00 MeV, in the intervals: $\theta_{Lab} = 30^\circ$ to 160° and $\theta_{Lab} = 40^\circ$ to 169° respectively, in steps of 10°. At these energies contributions from resonant scattering vanish.

The detection system consisted of three surface barrier detectors, positioned 10° apart, each of which subtended a solid angle of about 1 msr. The resolution of the detectors was improved by water cooling them to $0^\circ C$.

The targets were prepared by vacuum evaporation of 86% enriched ^{144}Sm, from a mixture of Sm_2O_3 and La, allowing the simultaneous evaporation of Sm and reduction of La to La_2O_3. The target thicknesses were of nominally 300 and 200 $\mu g/cm^2$. The thicker targets were used for the measurements at 14.00 MeV thus mantaining the energy loss in the target at about 5 keV for all bombarding energies. The overall energy resolution was about 25 keV . The absolute cross-section normalization, accurate to about 5%, was determined from the elastic scattering data by comaprison to optical model cross-section calculations at forward angles where the optical model is a small correction to Rutherford scattering. The errors bars on the data points indicate only statistical error.

III. ANALYSIS OF THE EXPERIMENTAL DATA.

The analysis consisted of two parts. First the non-resonant (background) scattering was studied at off-resonance energies and then used as a basis to extract an inter-polated background in the analysis of the resonance.

The data at 8.5 MeV and 14.0 MeV allowed the analysis of the non-resonant scattering. From the elastic scattering we determined the optical potential parameters and their energy dependence. These parameters were also tested in the analysis of the inelastic scattering data. In addition "best values" for the deformation parameters involved in the description of the direct inelastic scattering were obtained from the literature. Since at 8.5 MeV few neutron channels are open for the compound nucleus decay, a significant contribution in the proton channels is present (neutron threshold ∿ 7 MeV).

Fits of the elastic angular distributions at 14.0 MeV and 8.5 MeV, using the optical potential parameters listed in Table 1 are shown in Fig. 1. Initial values for the optical parameters were obtained from Ref[3,11] and the fits were done using the optical model code MAGALI[12]. The measured backangle cross sections at 8.5 MeV are somewhat higher than the shape elastic prediction, since fluctuating processes are contributing. Such processes should be even more pronounced in the inelastic cross sections. With the assumption of a linear energy dependence for the real potential depth, V,

we obtained the relation

$$V = -0.55\ E_p + 59.6\ \text{MeV},$$

where E_p is the incident particle energy in the Lab frame. The surface imaginary potential depth, W_S, was assumed to be independent of the energy.

The inelastic background comes from both direct and fluctuating processes. The direct inelastic scattering can be described as resulting from the excitation of the surface vibrational modes of the spherical target nucleus ^{144}Sm. This kind of scattering is essentially characterized by the deformation lengths

$$\delta_\lambda = \beta_\lambda R,$$

where β_λ is the deformation parameter for the vibrational mode λ. For each radius of the optical potential (Coulomb R_C, real volume R_N, surface imaginary R_S) a corresponding deformation parameter (β_λ^C, β_λ^N, β_λ^S) is defined, such that

$$\delta_\lambda = \beta_\lambda^N R_N = \beta_\lambda^C R_C = \beta_\lambda^S R_S.$$

The deformation lengths are already available in the literature from analyses of inelastic angular distributions at several

energies[13-16]. For the 2_1^+ state several δ_2-values, which differ significantly with each other, have been reported. Comparison between the experimental inelastic angular distribution at 14 MeV and coupled channels calculations, using ECIS code[17], showed that the best agreement is achieved with the δ_2-value of Larson et al (δ_2 = 0.46 fm)[16]. The result for this value of δ_2 is ilustrated in Fig.2.

Fig. 2 also shows the 8.5 MeV experimental inelastic angular distribution compared to that calculated for δ_2 = 0.46 fm Here the fluctuation contribution accounts for most of the cross section. At this energy only the neutron and proton channels are significant for compound nucleus decay. A Hauser-Feshbach (H.F.) calculation for proton decay of the compound nucleus involves the ^{144}Sm and ^{144}Eu optical potentials and the levels and level density parameters of these same nuclei. Level density estimates are always uncertain and information on the low lying states of ^{144}Eu, on which a H.F. calculation critically depends, is sparce. As a consequence the predictions of H.F. calculations in our work are reliable only in order of magnitude and the H.F. contribution was taken as an additive isotropic cross section to be treated as a fitting parameter in the inelastic slattering analysis. The validity of this rests on the isotropy of the H.F. contribution in the proton channel. For protons the combined centrifugal and Coulomb barriers drastically inhibit the partial waves with $\ell \neq 0$.

Taking $\sigma^{fl} \simeq 0.17$ mb/sr nicely fits the 8.5 MeV inelastic data as is shown in Fig. 2.

The 4_1^+ and 2_2^+ states may be interpreted as being built up from two harmonic quadrupole phonons. This description is illustrated in Figures 3a and 3b and has been used in a coupled channels calculation (ECIS), with $\delta_2 \simeq 0.46$ fm, at 30 MeV, since at this energy it is possible to compare the results with the data of Larson et al.[16]. The calculated cross sections were about 50 times smaller than the measured ones. This fact indicates that the anharmonic effects, shown in Fig. 3c which are not included in the coupled channels calculation, should play an important role. These effects can be taken into account by introducing new "effective" deformation parameters β_4' and β_2' and treating the 4_1^+ and 2_2^+ states as one phonon excitations, corresponding to the new effective amplitudes (see Figures 3d and 3e). Within this approach, that was adopted throughout this work, the experimental data were well described. The deformation lengths for all the studied states are presented in Table 3.

Neglecting the fluctuating contribution to the cross section, the scattering at the resonances energies is described through the scattering matrix:

$$S_{cc'} = S^{dir}_{cc'} - e^{i(\phi_c+\phi_{c'})} \sum_{\nu} \frac{g(J_\nu c)\, g(J_\nu c')}{E - E_{J_\nu} + \frac{i}{2}\Gamma_{J_\nu}} \quad , \qquad (3.1)$$

where $c \equiv \{\ell,j,I\}$, with $\{\ell,j\}$ the orbital and total angular momenta of the incident proton and I the spin of the larget; J_ν is the spin of the ν-th resonance; $\phi_c = \zeta_c + \sigma_c + \psi^R_c$, where ζ_c is the real optical model phase shift, σ^R_c the Coulomb phase shift and ψ^R_c the resonance mixing or asymmetry phase; E_{J_ν} and Γ_{J_ν} are the energy and total width of the J_ν- resonance, respectively. The resonance (or escape) amplitudes, $g(J_\nu c)$, are related to the spectroscopic amplitudes, $\theta(c, J_\nu)$, and partial widths, $\Gamma_{J_\nu,c}$, through the relations

$$\theta(c,J_\nu) = \frac{g(J_\nu,c)}{g^{sp}(J_\nu,c)} \qquad (3.2)$$

and

$$\Gamma_{J_\nu,c} = |g(J_\nu,c)|^2 \quad , \qquad (3.3)$$

where $g^{sp}(J_\nu,c)$ are the single particle amplitudes in channel c, at the J_ν- resonance energy.

The direct amplitude $S^{dir}_{cc'}$ was determined from the analysis of the off-resonance data presented in the previous section. The fit of the elastic cross section involves as parameters only the elastic partial width $\Gamma^0_{J_\nu}$, the energy E_{J_ν} and total width Γ_{J_ν} of the resonance. With these parameters determined from the analysis of elastic scattering the remaining parameters, in the inelastic angular distributions fits, were the inelastic partial widths. The fluctuating contribution to the cross section was obtained as a fitted additive parameter to the cross section described by the S matrix.

The fluctuating contributions to the elastic cross section at the resonance energies were estimated through Hauser-Feshbach calculations, using the code CINDY[18]. We have used the level density parameters of Gilbert and Cameron[19] and the optical potential of Bechetti and Greenlees[20] for ^{144}Eu. It turned out that in all the cases the elastic fluctuating cross section was of the same order of magnitude as the experimental error, and hence was disregarded.

The elastic scattering at the resonances of interest has been extensively studied. This fact enabled us to employ the resonance parameters available in the literature[1-4]. The best choice of resonance parameters, E_{J_ν}, Γ_{J_ν}, and elastic partial widths, $\Gamma_{J\nu}$, was determined through the reanalysis of the 170° elastic excitation function of Marouchian et al.[1]. It was also possible to determine the asymmetry phases during this procedure. The code ANSPEC[21] was employed in calculating the excitation function. The resulting fits can be seen in Fig. 4 and the corresponding final parametrization is presented in Table 3. These same parameters were used to calculate the elastic angular distributions shown with

the measured cross-sections in Fig. 5. From these angular distributions a determination was made of the difference

$$\Delta E = E_{J_\nu} - E \qquad (3.4)$$

where E is the beam energy during the experiment. The value of ΔE was varied within a 5 keV interval (the uncertainty in localizing the resonances) and the ΔE value which provided the best descriptions of the experimental angular distributions was the one adopted (see Table 3).

The H.F. calculation of the inelastic fluctuating contribution indicated that this process is relevant only at the two first resonances energies ($7/2_1^-$ and $3/2_1^-$). Its omission results in distortions in the fits as will be illustrated later on. As before, these contributions are treated as a free additive parameter to the cross section obtained from the scattering matrix .

The direct amplitude was obtained by the code JUPITOR [22] employing the parametrization defined in the analysis of the non-resonant data. Modifications were made to JUPITOR so that COULOMB excitation could be included in the 4_1^+ background amplitude. The optical phases were calculated with the code ANSPEC[21].

The angular distributions to the 2_1^+ , 4_1^+ and 2_2^+ states of ^{144}Sm were fitted at the four resonances. The analysis of the 3_1^- angular distributions was carried out only at the first resonance, since at the remaining energies the data

were masked by contaminants. Besides the parameter introduced to account for the fluctuating contribution the only free parameters still undetermined for these fits were the inelastic partial amplitudes $\Gamma_{J_\nu,c}$. Initial parameters were estimated for each of four resonances (Calculation I in section 4). Search for best parameters was made at each resonance, using a modified JUPITOR code. During this procedure, for a particular resonance the parameters previously obtained for the remaining resonances were included in the calculations. Reiteration through the set of resonances was continued until the values of the parameters stabilized. The resulting values are presented in Tables 4 to 7. The corresponding fits are compared to the data in Figs. 6 to 9. The fits are satisfactory at all the resonances and it can be seen from these figures that the experimental data of the $7/2^-$ and $3/2^-$ resonances are frequently better reproduced by inclusion of the fluctuating cross section. In particular, the improvement of the fit obtained by considering the fluctuating contribution in the case of the 2_1^+ state at the $7/2_1^-$ resonance is especially remarkable. This is consoling since major fluctuating contribution was expected in just this state.

The determination of the spectroscopic amplitudes from experimental values of $g(J_\nu,c)$ involves the calculation of single particle escape amplitudes $g^{sp}(J_\nu,c)$. As was extensively discussed by Harney and Weidenmüller[5] , the different approaches for g^{sp} available in the literature[6-9]

lead to considerablely different results. In the present work the single particle escape amplitudes were calculated using four different methods: Thompson, Adams and Robson[6] (TAR); Zaidi, Darmodjo and Harney[7,8] (ZDH); Mac Donald and Mekjian[9] and de Toledo Piza[10]. The results obtained with the two first methods are shown as a function of the emerging proton energy in Fig. 10. The method of de Toledo Piza gives results which are systematically about 10% greater than those obtained with the ZDH method, while the method of Mac Donald and Mekjian provides g^{sp} values which are always much smaller than that obtained with TAR method. It should be pointed out that the differences between the values furnished by the various methods are accentuated as the energy of the scattered proton increases. In other words, as the energy approaches that of the elastic scattering at the resonances of interest ($\sim$ 10 MeV), the discrepancies increase, and therefore the elastic amplitude, $\theta(\ell j,\ I=0,\ J_\nu)$, turns out to be the most affected one.

Tables 8 to 11 present the spectroscopic amplitudes that result from the experimental values of the inelastic partial widths (both with and without considering fluctuating contributions) and from the values of single particle escape widths obtained with the TAR and ZDH methods. In fact, considerable differences arise for $\theta(\ell j,0^+,J_\nu)$ as a consequence of using the approaches of TAR or ZDH. These difference become less significant as we consider increasingly excited core states.

The sum rule,

$$\sum_{\ell j,I_n} \theta^2(\ell j,I_n,J_\nu) \leq 1 \quad , \qquad (3.5)$$

was used as a consistency test for the analysis and for the calculations of g^{sp}. Table 12 presents the values of $\sum_{\ell j,I_n}\theta^2$ corresponding to the results showed in Tables 8 to 11. It is observed that, when the single particle escape widths calculated with the TAR method are employed, the condition (3.5) is only fulfiled for the $5/2^-$ state. The inclusion of the fluctuating contribution reduces the value of $\sum_{\ell j,I_n}\theta^2$, but the difficulty still subsists. The situation is greatly improved when the ZDH method is used; in this case the sum rule (3.5) is satisfied for all the states. It should be stressed, however, that the sum rule test cannot throw light on the necessity of including the fluctuating contribution. This may be understood by observing that the reduction of the spectroscopic amplitude for the core ground state, in general the largest one, is what allows the sum rule to be observed when employing g^{sp} values obtained with the ZDH method. Thus the test looses its sensitivity to the small values of spectroscopic amplitudes associated with the core excited states and these are the ones which are affected by the inclusion of fluctuating contributions.

We should remark that employing the g^{sp} values calculated through the method of de Toledo Piza the sum rule is still obeyed and the resulting values of $\theta(\ell j,I_n,J^\pi_\nu)$ are similar to that obtained with the ZDH method.

V. CALCULATIONS AND DISCUSSION

Theoretical spectroscopic amplitudes were obtained by discribing the nucleus ^{145}Sm in the particle-vibrator model. The simpler approach of a harmonically vibrating liquid drop was first adopted for the vibrator (Model I). Subsequently, the quasi-particle random phase approximation (QRPA) was employed (Model II); it is supposed that the residual interaction consists of a pairing force plus a separable multipolar interaction.

A - Model I: Particle-Vibrator Model with a Liquid Drop Vibrator

The Hamiltonian for the nucleus ^{145}Sm is written:

$$H = H_{vib} + H_{sp} + H_{int} \tag{4.1}$$

where H_{vib} describes the liquid drop ^{144}Sm:

$$H_{vib} = \sum_{\lambda} \hbar\omega_{\lambda} \left[N_{\lambda} + \frac{1}{2}(2\lambda+1)\right] \tag{4.2}$$

with $\hbar\omega_{\lambda}$ and N_{λ} the energy and number of phonons with multipolarity λ. The single-particle Hamiltonian H_{sp} in the occupation representation is given by:

$$H_{sp} = \sum_{jm} \varepsilon_j \, a^{+}_{jm} \, a_{jm} \quad , \tag{4.3}$$

where $a^{+}_{jm}(a_{jm})$ is the criation (anihilation) operator of a neutron in the jm orbital, j and m beeing respectively the angular momentum and its projection in the z-axes, and ε_j are the eigenvalues of H_{sp}. The interaction, H_{int}, between the particle and the vibrator is represented by

$$H_{int} = -\sum_{\lambda=2}^{3} \left(\frac{\hbar\omega_{\lambda}}{2C_{\lambda}}\right)^{1/2} \sum_{\mu=-\lambda}^{\lambda} (b_{\lambda\mu} + (-)^{\lambda+\mu} b^{+}_{\lambda-\mu}) \sum_{\substack{j_1 m_1 \\ j_2 m_2}} \langle j_1 m_1 | i^{\lambda} k_{\lambda}(r) Y_{\lambda\mu}(\vec{r}) | j_2 m_2 \rangle a^{+}_{j_1 m_1} a_{j_2 m_2} \quad , \tag{4.4}$$

where C_{λ} is the mass parameter of the vibrator;

$b^{+}_{\lambda\mu}$ is the creation (anihilation) operator of a phonon with multipolarity λ;

$|jm\rangle$ are the eigenfunctions of H_{sp},

$k(r)$ represents the radial dependency of the interaction and $Y_{\lambda\mu}(\vec{r})$ are spherical harmonics.

The relation between C_{λ} and the deformation parameter β_{λ} introduced in the last section, is given by

$$\beta_{\lambda} = \left[(2\lambda+1)\left(\frac{\hbar\omega_{\lambda}}{2C_{\lambda}}\right)\right]^{1/2} \tag{4.5}$$

The eigenfunctions of the total Hamiltonian are obtained treating H_{int} as a perturbation and adopting the unperturbed basis

$$|j(N_2 I_2 N_3 I_3) I, JM\rangle = \sum_{m M_I} (jmIM_I | JM) |jm\rangle |N_2 I_2 N_3 I_3, IM_I\rangle \tag{4.6}$$

The vector $|N_2 I_2 N_3 I_3, IM_I\rangle$ represents the state of the vibrator with N_2 quadrupole phonons coupled to I_2 and N_3 octupole phonons coupled to I_3 where I_2 and I_3 are coupled to I. The coeffiecients

of the expansion of the parent nucleus wave function, $|E^{\nu},JM\rangle$, in this basis are just the desired spectroscopic amplitudes:

$$|E^{\nu},JM\rangle = \sum C_{\nu}(j(N_2I_2N_3I_3)I;JM)|j(N_2I_2N_3I_3)I,JM\rangle \qquad (4.7)$$

and

$$\theta(\ell j,I,J_{\nu}) = C_{\nu}(j(N_2I_2,N_3I_3)I;JM) \qquad (4.8)$$

A calculation (Calculation I) within this model was carried out by allowing for the coupled neutron six single particle orbitals: $2f_{7/2}$, $1i_{13/2}$, $3p_{3/2}$, $3p_{1/2}$, $1h_{9/2}$ and $2f_{5/2}$, whose energies are presented in Table 13. For the radial matrix element, the estimation of Booth et al.[23], was adopted, viz,

$$\langle k(r)\rangle = 50 \text{ MeV} .$$

Core vibrational states with up to three quadrupole phonons ($N_2 \leq 3$) and up to two octupole phonons ($N_3 \leq 2$) were considered. The following experimental values of $\hbar\omega_{\lambda}$ and β_{λ} were employed (see previous section),

$$\hbar\omega_2 = 1.66 \text{ MeV} , \qquad \beta_2 = 0.070$$

$$\hbar\omega_3 = 1.81 \text{ MeV} , \qquad \beta_3 = 0.108$$

All basis vectors with unperturbed energies smaller than 7.0 MeV

were considered.

This model provides us with no information about the microscopic structure of the core (particle-hole excitations). Furthermore, it is implicity assumed that the 4_1^+ and 2_2^+ states correspond to two quadrupole phonons excitations, which is perhaps too strong a supposition. As a consequence the corresponding amplitudes in the parent wave functions are expected to be too small.

B - Model II: Quasi-Particle Random Phase Approximation

In this model we start with a microscopic shell model Hamiltonian,

$$H = H_{sp} + H_{res} , \qquad (4.9)$$

in which the residual interaction, H_{res}, involves a short range component represented by the pairing force and a long range component represented by multipolar interactions. The QRPA treatment of this problem has been discussed in detail by Ruiz et al.[24] and we refer the reader to this work for a detailed review and notation. Here we only describe our calculations for ^{144}Sm and ^{145}Sm nuclei.

The multipolar interaction constant χ_{λ} is given by the secular equation

$$\chi_{\lambda}^{-1} = -\frac{1}{2}\sum_{j_1j_2}\left[P(j_1j_2\lambda)\right]^2\left[\frac{1}{E_{j_1}+E_{j_2}-\hbar\omega_{\lambda,i}} + \frac{1}{E_{j_1}+E_{j_2}+\hbar\omega_{\lambda,i}}\right] . \qquad (4.10)$$

were

$$E_j = \left[(\varepsilon_j - \varepsilon_F)^2 + \Delta^2 \right]^{1/2} , \qquad (4.11)$$

are the independent quasiparticle energies; ε_F is the chemical potential and Δ represents the energy gap. The quantity $P(j_1 j_2 \lambda)$ is defined as

$$P(j_1 j_2 \lambda) = (2\lambda+1)^{-\frac{1}{2}} (U_{j_1} V_{j_2} + U_{j_2} V_{j_1}) \langle j_1 || i^\lambda r^\lambda Y_\lambda || j_2 \rangle , \qquad (4.12)$$

where U_j and V_j are, respectively, the vacancy and occupation numbers. For a given value of χ_λ the secular equation (4.10) presents several roots, $\hbar\omega_i$ (assigned by i), corresponding to the same λ and different $\Lambda_{\lambda,i}$, given by

$$\Lambda_{\lambda,i}^{-2} = \frac{\partial}{\partial(\hbar\omega_{\lambda,i})} \left[\chi_\lambda^{-1}\right] = \frac{1}{2} \sum_{j_1 j_2} \left[P(j_1 j_2 \lambda)\right]^2 \left[\frac{1}{(E_{j_1}+E_{j_2}+\hbar\omega_{\lambda,i})^2} - \right.$$

$$\left. - \frac{1}{(E_{j_1}+E_{j_2}-\hbar\omega_{\lambda,i})^2}\right] \qquad (4.13)$$

The QRPA formalism allows us to consider the two 2^+ core states as corresponding to two distinct one-phonon excitations (one collective, the other not) with amplitudes given by the first two roots of the secular equation. The 3_1^- and 4_1^+ states were also treated as one-phonon excitations.

Figure 11 shows the behaviour of χ_λ and Λ_λ as a function of $\hbar\omega_\lambda$, for λ = 2, 3 and 4. These functions were calculated with the single particle energies for protons and neutrons taken from Refs. 25-27 and listed in Table 13. Harmonic oscillator wave functions were used in the calculation of the radial matrix elements of the interaction.

Solutions of the gap equations for the protons (open shell), with Δ = 1.26 MeV obtained from binding energies[28], simultaneously furnished the values for ε_F and G:

$$\varepsilon_F = 3.20 \text{ MeV} ,$$

$$G = 0.132 \text{ MeV} .$$

The condition that the solutions of (4.10) correspond to the experimental energies of the 2_1^+, 3_1^- and 4_1^+ states result in the values of the multipole interaction constant χ_λ, presented in Table 14. From this value of χ_2 the second root, $\hbar\omega_{2,2}$ = 2.62 MeV, was obtained which corresponded closely to the experimental value 2.42 MeV. Table 14 also shows the amplitudes represented by $\Lambda_{\lambda,i}^{th}$. These quantities can also be estimated from the experimental values of β_λ, presented in the previous section, through the relation

$$\Lambda_\lambda = \frac{\langle k \rangle}{\langle r^\lambda \rangle} \frac{\beta_\lambda}{(2\lambda+1)^{1/2}} \qquad (4.14)$$

Using $\langle k \rangle$ = 50 MeV and $\langle r^\lambda \rangle = \left[3/(3+\lambda)\right] R^\lambda$, with R = 1.2 $A^{1/3}$ fm (A = the mass number of the nucleus), relation (4.14) provides us with the empirical values of the amplitudes, $\Lambda_{\lambda,i}^{emp}$, listed in Table 14. From the table we note that both estimates give similar values for Λ_3 and Λ_4. On the other hand, $\Lambda_{2,1}^{th}$ is considerably greater than $\Lambda_{2,1}^{emp}$, while $\Lambda_{2,2}^{th}$ is significantly smaller than $\Lambda_{2,2}^{emp}$. Thus one concludes that the QRPA model well describes the structure of the 3_1^- and 4_1^+ states but furnishes too much collectivity to the 2_1^+ state at the expenses of the 2_2^+ state. To account for this effect we employed the empirical.

values of $\Lambda_{2,1}$ and $\Lambda_{2,2}$. Moreover, up to two quadrupole phonons of the first kind were considered, while for the other vibrational fields only one phonon states were taken into account. The results obtained within this framework will be labeled as Calculation II.

Another calculation (Calculation III) was performed within the QRPA model using the same configuration space and the same parametrization as in the previous case, except that here we have employed the empirical values of the energies $\hbar\omega_\lambda$ and of the coupling constants Λ_λ. Furthermore, in this case we used the estimate $\langle k \rangle = 50$ MeV.

In both QRPA calculations the spectroscopic amplitudes were evaluated by means of Eq. (4.23) of Ref. 24.

Figure 4 compares the ^{145}Sm spectrum obtained from the above mentioned calculations with the experimental one[4]. It is observed that the low energy spectrum is always well reproduced with the exception of the $1/2_1^-$ state, which lies too low in energy within the two later calculations. The better agreement with the experimental data achieved with the first calculation is ascribed to the utilization of single-particle energies of Heyde et al[26], which were obtained by fitting the low energy spectrum, within model I.

The calculated spectroscopic amplitudes are presented in Tables 8 to 11, where they can be compared to their experimental values. All three calculations provided similar values for the spectroscopic amplitudes associated with elastic scattering $\theta(\ell j, 0^+, J_\nu^\pi)$ and, in general, a reasonable agreement with the ex-

perimental values was obtained.

The amplitudes associated with the 2_1^+ state, $\theta(\ell j, 2_1^+, J_\nu^\pi)$, resulting from different calculations are quite similar, reflection the equivalency among the corresponding model descriptions. For $J_\nu^\pi = 3/2_1^-$, $1/2_1^-$ and $5/2_1^-$ levels a satisfactory agreement between theoretical and experimental results is obtained. One should note however that, although an agreement is observed within the experimental errors for the $1/2_1^-$ state, the theory predicts in this case a major contribution of the component with $\ell j = p_{3/2}$ relative to the $f_{7/2}$ component, while the experimental results show an inverse behaviour. In the case of the $7/2_1^-$ state the theoretical and experimental values of $\theta(f_{7/2}, 2_1^+, 7/2_1^-)$ disagree significantly with each other when the fluctuating contribution is neglected. Inclusion of this process affects mostly only the forgoing amplitude, reducing it to half of its previous value. The resulting agreement then achieved between theoretical and experimental values is quite satisfactory.

Within Model I it is not possible to account for the inelastic scattering to the 3_1^- state. On the other hand, Calculations II and III, performed within the QRPA framework, give rise to quite similar results for the theoretical amplitudes $\theta(s_{1/2}, 3_1^-, 7/2_1^-)$ and $\theta(d_{3/2}, 3_1^-, 7/2_1^-)$, which agree with the experimental data.

The description of the 4_1^+ state is different in each calculation. As it was expected calculation I provides too small amplitudes, especially for the $7/2_1^-$ and $3/2_1^-$ states. In addition, no one of the calculations was able to reproduced the signs of the spectroscopic amplitudes for the $5/2_1^-$ state and Calculation II systematically furnishes amplitudes which are twice as large as those

of calculation III. It is this latter calculation which best agrees with experiments. The $\theta(p_{3/2},4_1^+,7/2_1^-)$ amplitude agrees with Calculation I, when the fluctuating contribution is neglected. But, when this effect is included, the "experimental value" of the foregoing amplitude is reduced by a factor of two, thus falling into agreement with Calculation III.

The 2_2^+ state is very badly described within Model I, since the theoretical amplitudes turn out to be, in most cases, too small and with wrong signs in comparison with the experimental values. It should be stressed that inclusion of the fluctuating contribution for the core state is essential for getting an agreement between experimental and theoretical values. The amplitudes which are mostly affected (producing even the necessary changes in the signs) are $\theta(f_{7/2},2_2^+,7/2_1^-)$ and $\theta(p_{3/2},2_2^+,3/2_1^-)$. The inclusion of the fluctuating process is also responsable for the reduction of the $\theta(f_{7/2},2_2^+,3/2_1^-)$ and $\theta(p_{1/2},2_2^+,3/2_1^-)$ amplitudes and the increase of the $\theta(f_{7/2},2_2^+,3/2_1^-)$ amplitude producing in this way a good agreement between theoretical predictions and experimental values. Finally, for the $1/2_1^-$ state we observe that the theoretical amplitudes $\theta(\ell j,2_2^+,1/2_1^-)$ are close to the experimental values, while for the $5/2_1^-$ state none of the calculations was able to reproduce correctly the signs of the experimental amplitudes.

VI. CONCLUSION

From an analysis of proton angular distributions at four isobaric analog resonances of the ^{144}Sm + p system we have extracted spectroscopic informations about the corresponding low-lying states of the ^{145}Sm nucleus. Among these results

only those relative to the 0_1^+ and 2_1^+ core states have been available in the literature[1-4] and even these presented inconsistencies which were attributed to the adopted description of the background[4]. The data reported by Martin et al.[3] suggested to us that configurations involving the 3_1^-, 4_1^+ and 2_2^+ states of ^{144}Sm should be relevant in building up the parent state wave functions and this was confirmed by the corresponding spectroscopic information that was obtained for the first time in the present work.

An appreciable effort was invested in order to obtain a precise description of the background. The direct scattering was treated within the coupled channel approach which was preferable to the usual DWBA representation. The fluctuating contribution was also taken into account, and proved to be relevant at the first two resonances, especially for the scattering to the 2_1^+ and 2_2^+ states of ^{144}Sm.

The magnitudes of the spectroscopic amplitudes extracted from the experimental data depend, in addition, on the method employed in the estimate of the single-particle escape amplitudes. The analysis performed here suggests that the method of Zaidi, Damodjo and Harney[7,8] and that of Toledo Piza[10], could be more realistic that those of Thompson, Adams and Robson[6] and of Mac Donald and Mekjian[9].

The experimental spectroscopic amplitudes were compared to calculations based on the particle-vibrator model, with the vibrator approximated at first by a liquid drop, and then treated within the QRPA. With the last representation a good agreement was

always observed, while for the liquid drop vibrator this did not occur, especially for the 3_1^- and 2_2^+ core states. This showed the importance of considering the microscopic structure of the core. The agreement observed between the experimental and theoretical spectroscopic amplitudes when the fluctuating contribution is taken into account is quite impressive, pointing out the necessity of including this contribution in the description of the background for the ^{144}Sm + p system and giving credence to our procedure. It would be of interest to independently calculate the fluctuation contributions to the cross sections and so avoid the uncertainties arising from adjusting their values. However rigorous calculations require level information not presently available, and pose theoretical difficulties because of interaction between the analog resonances and the $T^<$ states responsible for the fluctuation cross-section.

ACKNOWLEDGEMENTS

We are deeply grateful to Elizabeth Farrelly Pessoa for a very careful reading of the manuscript and for very useful discussions. One of us, J.L.Foster, would like to thank the IPN, Orsay France and J.P. Schapira for their hospitality during a two month stay. IPN supplied the computer time for the preliminary reaction analysis. One of us (F.K.) is pleased to acknowledge many extremely helpful discussions with A.F.R. de Toledo Piza.

REFERENCES:

1. K. Marouchian, P. von Brentano, J.P. Wurm and S.A.A. Zaidi, Z. Naturforsch. 21a (1966) 929.
2. R.K.Jolly and C.F. Moore, Phys. Rev. 155 (1967) 1377.
3. R. Martin, L. Bimbot, S.Gales, L. Lessard, D. Spalding, W.G. Weitkamp, O. Dietzsch and J.L. Foster Jr., Nucl. Phys. A210 (1973) 221.
4. H. Clement, G. Graw, R. Zenger and G. Zöllner, Nucl. Phys. A285 (1977) 109.
5. H.L. Harney and H.A. Weidenmüller, Nucl. Phys. A139 (1969) 241.
6. W.J. Thompson, J.L. Adams and D. Robson, Phys. Rev. 173 (1968) 975.
7. S.A.A. Zaidi and S. Darmodjo, Phys. Rev. Lett. 19 (1967) 1446.
8. H.L. Harney, Nucl. Phys. A119 (1968) 591.
9. A. Mekjian, W.M. Mac Donald, Nucl. Phys. A121 (1968) 385.
10. A.F.R. de Toledo Piza, Instituto de Física, Universidade de São Paulo, Brazil, Technical Report TABU (unpublished).
11. F.G. Perey, Phys. Rev. 132 (1963) 755.
12. J. Raynal, Centre d'Études Nucleaires, Saclay, France Techical Report MAGADI (unpublished).
13. J.H. Barker and J.C. Hiebert, Phys. Rev. C4 (1971) 2256.

14. P.B. Woollan, R.J. Griffiths and N.M. Clarke, Nucl. Phys. A189 (1972) 321.

15. P.B. Woollan, R.J. Grifiths, J.L. Parish, J.G. Kulleck, R.F. Moore and P. von Brentano, Phys. Rev. 165 (1968) 1312.

16. D. Larson, S.M. Austin and B.H. Wildenthal, Phys. Rev. 175 (1968) 1482.

17. J. Raynal, Computing as a Language in Physics, IAEA (1972) 918.

18. E. Sheldon and V.C. Rogers, Comp. Phys. Commum. 6 (1973) 99.

19. A. Gilbert and A.G.W. Cameron, Can. Journ. Phys. 43 (1965) 1446.

20. F.D. Becchetti Jr. and G.W. Greenlees, Phys. Rev. 182 (1969) 1190.

21. W.J. Thompson, J.L. Adams, Technical Report ANSPEC, Tandem Accelerator Laboratory, Florida State University Tallassee (unpublished).

22. T. Tamura, Rev. Mod. Phys. 37 (1965) 679.

23. W. Booth, S. Wilson and S.S. Ipson, Nucl. Phys. A229 (1974) 61.

24. M.C.H.M. Ruiz, M.L. Cescato, J.L. Foster Jr. and F. Krmpotić (following paper).

25. H. Heyde, W. Warouquier and H. Vincx, Phys. Lett. 57B (1975) 429.

26. B.H. Wildenthal, E. Newman and R.L. Auble, Phys. Rev. 82 (1971) 690.

27. A. Covello, V.R. Manfredi and N. Azziz, Nucl. Phys. A201 (1973) 215.

28. A. Bohr and B.R. Mottelson, Nuclear Structure (W.A. Benjamin Inc., New York, 1969), Vol. I

FIGURE CAPTIONS:

Figure 1. Elastic angular distributions at 8.5 and 14.0 MeV. The form of the optical potential is $U(r)=V_C-V.f(r,R_N,a_N)-i\ W_S.\frac{d}{dr}f(r,R_S,a_S)+$ $+V_{SO}(\vec{\sigma}.\vec{\ell})(\frac{\hbar}{m_\pi c})^2\frac{1}{r}\frac{d}{dr}f(r,R_{SO},a_{SO})$, where f(r,R,a) is the usual Saxon-Woods form. The parametrization corresponding to the fits is presented in Table 1.

Figure 2. Inelastic angular distribution of the cross section for the 2_1^+ state at 8.5 and 14.0 MeV. The solid curves correspond to the total cross section. At 14.0 MeV only direct processes contribute and the curve corresponds to the coupled channel calculation with δ_2 = 0.46 fm. At 8.5 MeV the solid curve results from adding the direct contribution calculated in the same way (dashed line) to the fitted compound nucleus contribution (0.17 mb/sr).

Figure 3. Grafical representation of the excitation mechanism for the 2_2^+ and 4_1^+ two-quadrupole phonon states. Within Model I, which does not include the anharmonic effects, the 2_2^+ and 4_1^+ states are attained only via two-steps processes shown in graph (a). However, when one considers also the contributions from the second derivative of the optical potential, the term gives rise to the excitations sketched in graph (b). Diagram (c) shows the excitation of the two-quadrupole phonon states through the anharmonic effects induced by the particle-phonon coupling. This type of excitation of the 2_2^+ and 4_1^+ states can be simulated by effective λ=2 and λ=4 vibrational fields as illustrated in graphs (d) and (e), respectively.

Figure 4. Fits to 170° elastic excitation function over the 4 analysed resonances. The corresponding parametrization is presented in Table 3.

Figure 5. Resonant elastic angular distributions. The parametrization corresponding to the fits is presented in Table 3.

Figure 6. Fits to the resonant angular distributions for the 2_1^+ state. For the $7/2_1^-$ and $3/2_1^-$ resonances the dashed (solid) lines correspond to the fits obtained by disregarding (considering) the fluctuating contribution.

Figure 7. Fit to the resonant angular distribution for the 3_1^- state at the $7/2_1^-$ resonance. The dashed (solid) line correspond to the fit obtained by disregarding (considering) the fluctuating contribution.

Figure 8. Fits to the resonant angular distribution for the 4_1^+ state. For the $7/2_1^-$ and $3/2_1^-$ resonances the dashed (solid) lines correspond to the fits obtained by disregarding (considering) the fluctuating contribution.

Figure 9. Fits to the resonant angular distribution for the 2_2^+ state. For the $7/2_1^-$ and $3/2_1^-$ resonances the dashed (solid) lines correspond to the fits obtained by disregarding (considering) the fluctuating contribution.

Figure 10. Single particle escape amplitudes calculated by the methods of TAR[6] (solid lines) and ZDH[7,8] (dashed lines) as a function of the emerging proton energy.

Figure 11. Behaviour of the functions $S_\lambda(\omega)$ and $\Lambda_\lambda(\omega)$ as a function of the energy $\hbar\omega_\lambda$ near the first roots of the secular equation (4.10); $\hbar\omega_2$ = 1.66 and 2.62 MeV, $\hbar\omega_3$ = 1.81 MeV, $\hbar\omega_4$ = 2.19 MeV. The dashed vertical lines indicate the unperturbed energies of two quasiparticles.

Figure 12. Experimental[4] and calculated energy levels of ^{145}Sm. The spectra indicated by (1), (2) and (3) were obtained by Calculations I, II and III respectively.

TABLE 1. Optical model parameters. The real potential depth is given by $V = V_o \times E_p$ MeV, where E_p is the incident particle energy in the Lab frame.

V_o (MeV)	κ	R_R (fm)	a_R (fm)	W_S (MeV)	R_S (fm)	a_S (fm)	V_{so} (MeV)	R_{so} (fm)	a_{so} (fm)	R_C (fm)
59.60	0.55	6.552	0.7113	9.02	6.709	0.6703	6.2	5.766	0.7113	6.290

TABLE 2. Deformation lengths for ^{144}Sm states. The δ_λ values are taken from Ref. 16.

I_n^π	$E_{excit.}$ (MeV)	λ	δ_λ (fm)
2_1^+	1.661	2	0.46
3_1^-	1.811	3	0.87
4_1^+	2.191	4	0.33
2_2^+	2.423	2	0.29

TABLE 3. Resonance parameters and elastic partial widths. The quantity ΔE is defined as the difference between the beam and resonance energies (Lab frame). The parameters of those resonances marked by * were taken from Ref. 4 and used in background for the other resonances (see Fig.4). The $7/2_1^-$ resonance energy (9.251 MeV) is taken from Ref.3. The energies of the $3/2_1^-$, $1/2_1^-$ and $5/2_1^-$ resonances are relative to 9.251 MeV.

J_ν^π		$E_{RES}^{J\nu}$ (CM) (MeV)	$\Gamma_T^{J\nu}$ (keV)	Γ_J^o (keV)	ψ_ℓ	ΔE (keV)
$7/2_1^-$		9.251	49	7.8	0^o	0
$3/2_1^-$		10.135	70	22.0	8^o	0
$9/2_1^-$	*	10.690	47	0.7		
$1/2_1^-$		10.835	90	31.5	8^o	-5
$5/2_1^-$		10.904	51	4.1	0^o	5
$9/2_2^-$	*	11.040	50	0.3		
$7/2_2^-$	*	11.120	36	1.7		
$3/2_2^-$	*	11.220	52	9.7		
$5/2_2^-$	*	11.240	45	6.9		

TABLE 4. Partial widths for the $7/2_1^-$ resonance. All the widths are given in keV unities. The values obtained by disregarding the fluctuating contribution are indicated by (I). Those obtained by including this contribution are indicated by (II).

I_n	$\Gamma(s_{1/2}, I_n)$	$\Gamma(d_{3/2}, I_n)$	$\Gamma(f_{7/2}, I_n)$	$\Gamma(p_{3/2}, I_n)$	$\Gamma(p_{1/2}, I_n)$	$\Gamma(f_{5/2}, I_n)$	σ_{BC} (mb/sr)
0_1^+	.....	.....	7.8±0.8	.....	.....	.....	———
2_1^+ (I)	.....	.....	0.58±0.05	0.40±0.06	.....	0.001±0.06	———
2_1^+ (II)	.....	.....	0.13±0.06	0.41±0.04	.....	0.003±0.01	0.13±0.03
3^- (I)	0.77±0.06	0.05±0.03	.....	.....	.....	.....	———
3^- (II)	0.86±0.07	0.04±0.01	.....	.....	.....	.....	0.03±0.01
4_1^+ (I)	.....	.....	0.11±0.03	0.11±0.03	0.005±0.02	0.003±0.01	———
4_1^+ (II)	.....	.....	0.15±0.01	0.03±0.01	0.004±0.01	———	0.025±0.002
2_2^+ (I)	.....	.....	0.03±0.03	0.14±0.03	.....	0.03 ±0.01	———
2_2^+ (II)	.....	.....	0.003±0.01	0.04±0.01	.....	0.08 ±0.01	0.025±0.007

TABLE 5. Partial widths for the $3/2_1^-$ resonance. All the widths are given in keV unities. The notation is the same as in Table 4.

I_n	$\Gamma(f_{7/2}, I_n)$	$\Gamma(p_{3/2}, I_n)$	$\Gamma(p_{1/2}, I_n)$	$\Gamma(f_{5/2}, I_n)$	σ_{BC} (mb/sr)
0_1^+	.....	32±2	.....	.....	———
2_1^+ (I)	2.49±0.2	0.41±0.1	0.37±0.1	0.07±0.1	———
2_1^+ (II)	2.50±0.04	0.21±0.05	0.35±0.01	0.07±0.1	0.027±0.007
4_1^+ (I)	0.09±0.02	.....	.....	0.003±0.01	———
4_1^+ (II)	0.07±0.02	.....	.....	0.0008±0.001	0.006±0.004
2_2^+ (I)	0.003±0.02	0.006±0.1	0.37±0.03	———	———
2_2^+ (II)	0.009±0.01	0.24 ±0.03	0.01±0.01		0.012±0.005

TABLE 6. Partial widths for the $1/2_1^-$ resonance. All the widths are given in keV unities. The notation is the same as in Table 4.

I_n	$\Gamma(f_{7/2}, I_n)$	$\Gamma(p_{3/2}, I_n)$	$\Gamma(p_{1/2}, I_n)$	$\Gamma(f_{5/2}, I_n)$
0_1^+	.....	.....	31.5±4	.....
2_1^+	.....	1.33±0.6	.....	5.08±0.8
4_1^+	1.38±0.4	.....	.....	.....
2_2^+	.....	0.36±0.04	.....	0.14±0.05

TABLE 7. Partial widths for the $5/2_1^-$ resonance. All the widths are given in keV unities. The notation is the same as in Table 4.

I_n	$\Gamma(f_{7/2}, I_n)$	$\Gamma(p_{3/2}, I_n)$	$\Gamma(p_{1/2}, I_n)$	$\Gamma(f_{5/2}, I_n)$
0_1^+	.....	.....	.....	4.1±1
2_1^+	8.62±0.5	0.53±0.5	0.41±0.2	0.33±0.05
4_1^+	0.20±0.04	0.001±0.001	.....	———
2_2^+	0.06±0.02	0.16±0.04	0.000±0.001	———

TABLE 8. Spectroscopic amplitudes for the $7/2^-_1$ state of ^{145}Sm.

The results obtained from the fits that disregard (consider) the fluctuating contribution are indicated by TAR (TARNC) when the single particle escape widths are evaluated with the TAR method[6] and by ZDH (ZDHNC) when they are calculated with the ZDH method[7,8]. We have indicated by CI, CII and CIII the model calculations I, II and III, respectively, which are described in the next section.

	I_n	$\theta(f_{7/2},I_n,7/2^-_1)$	$\theta(d_{3/2},I_n,7/2^-_1)$	$\theta(f_{7/2},I_n,7/2^-_1)$	$\theta(p_{3/2},I_n,7/2^-_1)$	$\theta(p_{1/2},I_n,7/2^-_1)$	$\theta(f_{5/2},I_n,7/2^-_1)$
TAR				0.84±0.10			
ZDH				0.75±0.08			
CI	0^+_1			0.91			
CII				0.86			
CIII				0.90			
TAR				-0.59±0.05	-0.20±0.03		0.03±0.2
ZDH				-0.48±0.04	-0.16±0.02		0.02±0.2
TARNC				-0.38±0.05	-0.20±0.02		0.05±0.2
ZDHNC	2^+_1			-0.23±0.05	-0.17±0.02		0.04±0.1
CI				-0.28	-0.15		-0.04
CII				-0.26	-0.14		-0.04
CIII				-0.26	-0.14		-0.04
TAR		-0.20±0.02	-0.09±0.04				
ZDH		-0.17±0.01	-0.08±0.03				
TARNC		-0.18±0.02	-0.09±0.02				
ZDHNC	3^-_1	-0.16±0.02	-0.08±0.02				
CI		———	———				
CII		-0.18	-0.11				
CIII		-0.19	-0.12				
TAR				0.36±0.06	0.13±0.02	0.03±0.1	0.04±0.2
ZDH				0.30±0.05	0.11±0.02	0.02±0.1	0.04±0.2
TARNC				0.43±0.03	0.07±0.02	0.03±0.06	
ZDHNC	4^+_1			0.35±0.02	0.05±0.02	0.02±0.06	
CI				0.04	0.02	0.02	0.01
CII				0.16	0.10	0.11	0.07
CIII				0.08	0.05	0.05	0.03
TAR				0.31±0.1	-0.17±0.03		0.24±0.1
ZDH				0.17±0.1	-0.14±0.03		0.20±0.1
TARNC				-0.03±0.08	-0.09±0.02		0.38±0.1
ZDHNC				-0.03±0.06	-0.07±0.02		0.32±0.1
	2^+_2						
CI				0.003	-0.04		0.008
CII				-0.08	-0.06		0.03
CIII				-0.09	-0.06		0.03

TABLE 9. Spectroscopic amplitudes for the $3/2^-_1$ State of ^{145}Sm. The notation is the same as in Table 8.

	I_n	$\theta(f_{7/2},I_n,3/2^-_1)$	$\theta(p_{3/2},I_n,3/2^-_1)$	$\theta(p_{1/2},I_n,3/2^-_1)$	$\theta(f_{5/2},I_n,3/2^-_1)$
TAR			0.81±0.07		
ZDH			0.81±0.05		
	0^+_1				
CI			0.71		
CII			0.67		
CIII			0.70		
TAR		-0.75±0.08	-0.15±0.04	-0.14±0.04	-0.13±0.3
ZDH		-0.60±0.05	-0.12±0.03	-0.13±0.03	-0.11±0.3
TARNC		-0.75±0.01	-0.11±0.03	-0.14±0.01	-0.13±0.3
ZDHNC		-0.61±0.01	-0.09±0.02	-0.11±0.01	-0.11±0.3
	2^+_1				
CI		-0.61	-0.18	-0.18	-0.08
CII		-0.55	-0.17	-0.16	-0.07
CIII		-0.59	-0.17	-0.18	-0.08
TAR		0.19±0.04			0.04±0.1
ZDH		0.16±0.04			0.03±0.1
TARNC		0.17±0.05			0.02±0.03
ZDHNC		0.14±0.04			0.02±0.02
	4^+_1				
CI		0.08			0.04
CII		0.23			0.16
CIII		0.12			0.08
TAR		-0.04±0.2	0.006±0.08	-0.18±0.01	
ZDH		-0.03±0.2	0.004±0.05	-0.15±0.01	
TARNC		-0.067±0.07	-0.15±0.03	-0.04±0.03	
ZDHNC		-0.055±0.06	-0.12±0.02	-0.03±0.03	
	2^+_2				
CI		0.14	0.05	0.05	
CII		-0.13	-0.06	-0.05	
CIII		-0.15	-0.06	-0.05	

TABLE 10. Spectroscopic amplitudes for the $1/2^-_1$ State of ^{145}Sm. The notation is the same as in Table 8.

	I_n	$\theta(f_{7/2}, I_n, 1/2^-_1)$	$\theta(p_{3/2}, I_n, 1/2^-_1)$	$\theta(p_{1/2}, I_n, 1/2^-_1)$	$\theta(f_{5/2}, I_n, 1/2^-_1)$
TAR				0.91±0.12	
ZDH				0.68±0.09	
	0^+_1				
CI				0.78	
CII				0.73	
CIII				0.77	
TAR			0.23±0.10		-0.64±0.2
ZDH			0.18±0.08		-0.52±0.1
	2^+_1				
CI			0.47		-0.29
CII			0.50		-0.23
CIII			0.55		-0.26
TAR		-0.86±0.08			
ZDH		-0.21±0.05			
	4^+_1				
CI		-0.24			
CII		-0.46			
CIII		-0.32			
TAR			0.14±0.03		-0.19±0.04
ZDH			0.11±0.01		-0.16±0.05
CI	2^+_2		-0.11		0.06
CII			0.10		-0.08
CIII			0.12		-0.10

TABLE 11. Spectroscopic amplitudes for the $5/2^-_1$ state of ^{145}Sm. The notation is the same as in Table 8.

	I_n	$\theta(f_{7/2}, I_n, 5/2^-_1)$	$\theta(p_{3/2}, I_n, 5/2^-_1)$	$\theta(p_{1/2}, I_n, 5/2^-_1)$	$\theta(f_{5/2}, I_n, 5/2^-_1)$
TAR					0.44±0.11
ZDH					0.36±0.09
	0^+_1				
CI					0.57
CII					0.50
CIII					0.45
TAR		0.87±0.19	0.15±0.1	-0.13±0.06	-0.17±0.04
ZDH		0.69±0.16	0.11±0.1	-0.10±0.04	-0.14±0.03
CI	2^+_1	0.83	0.12	-0.11	-0.10
CII		0.66	0.12	-0.10	-0.13
CIII		0.76	0.11	-0.14	-0.11
TAR		0.19±0.04	0.006±0.01		
ZDH		0.08±0.02	0.005±0.01		
CI	4^+_1	-0.15	-0.06		
CII		-0.17	-0.18		
CIII		-0.09	-0.08		
TAR		0.11±0.04	-0.09±0.02	0.001±0.04	
ZDH		0.08±0.03	-0.08±0.02	0.001±0.03	
CI	2^+_2	-0.07	-0.12	0.03	
CII		0.03	0.03	-0.05	
CIII		0.03	0.03	-0.06	

TABLE 12. The sum $\sum_{\ell j, I_n} \theta^2 (\ell j, I_n, J^\pi_\nu)$ for each studied state. The notation is the same as in Table 8.

	J^π_ν			
	$7/2^-_1$	$3/2^-_1$	$1/2^-_1$	$5/2^-_1$
TAR	1.60±0.36	1.35±0.33	1.41±0.30	1.08±0.20
ZDH	1.05±0.35	0.82±0.32	0.85±0.20	0.66±0.07
TARNC	1.39±0.27	1.32±0.24	———	———
ZDHNC	0.91±0.20	0.81±0.22	———	———

TABLE 13. Single particle energies for neutrons and protons. The gaps between the shells were obtained from the differences $Q_{\gamma n} - Q_{n\gamma}$ or $Q_{\gamma p} - Q_{p\gamma}$ for the corresponding closed shell nuclei (Q_{xy} represents the threshold for the (x,y) reaction). The values of $\varepsilon_{n\ell j}$ were taken from Refs. 25-27.

$n\ell j$	$\varepsilon^{sp}_{n\ell j}$(NEUTRONS) (MeV)	$\varepsilon^{sp}_{n\ell j}$(PROTONS) (MeV)
$2f_{5/2}$	2.250	8.94
$3p_{1/2}$	1.800	10.77
$3p_{3/2}$	1.210	9.49
$1h_{9/2}$	1.350	5.92
$1i_{13/2}$	1.500	8.30
$2f_{7/2}$	0.000	6.30
$2d_{3/2}$	-3.79	1.70
$3s_{1/2}$	-4.20	1.45
$1h_{11/2}$	-4.94	1.30
$2d_{5/2}$	-5.15	0.00
$1g_{7/2}$	-5.94	-0.70
$1g_{9/2}$	-10.56	-5.48
$2p_{1/2}$	-11.28	-5.58
$2p_{3/2}$	-12.57	-7.48
$1f_{5/2}$	-12.76	-7.98
$1f_{7/2}$	-15.75	-10.96

TABLE 14. Calculated values of the coupling constants, χ_λ, and theoretical and empirical values for the particle-phonon vertix amplitudes, Λ_λ.

λ	i	$\hbar\omega_{\lambda,i}$ (MeV)	$\chi_{\lambda,i}$ (MeV/fm$^{2\lambda}$)	$\Lambda^{th}_{\lambda,i}$ (MeV/fm$^{\lambda}$)	$\Lambda^{emp}_{\lambda,i}$ (MeV/fm$^{\lambda}$)
2	1	1.661	1.45×10^{-3}	0.074	0.053
3	1	1.811	2.94×10^{-5}	0.012	0.014
4	1	2.191	0.80×10^{-6}	0.0012	0.0011
2	2	2.67	1.45×10^{-3}	0.015	0.030

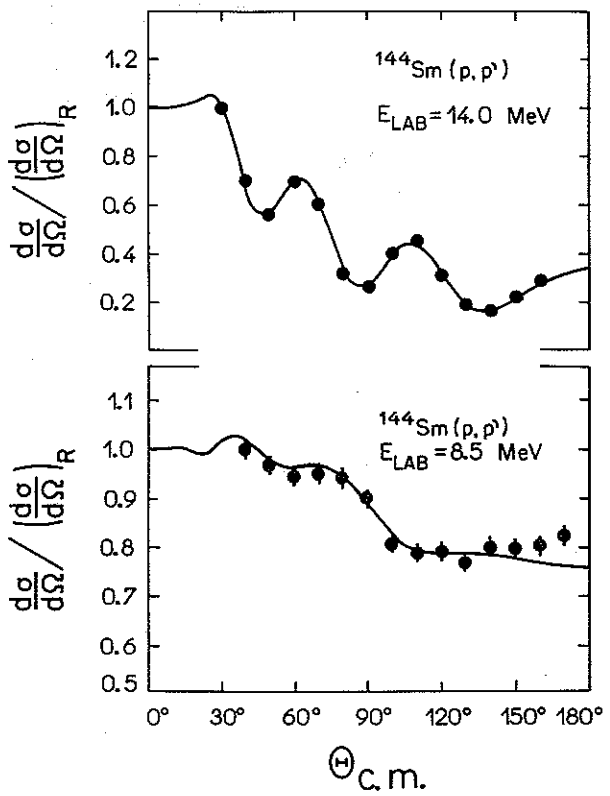

FIG. 1

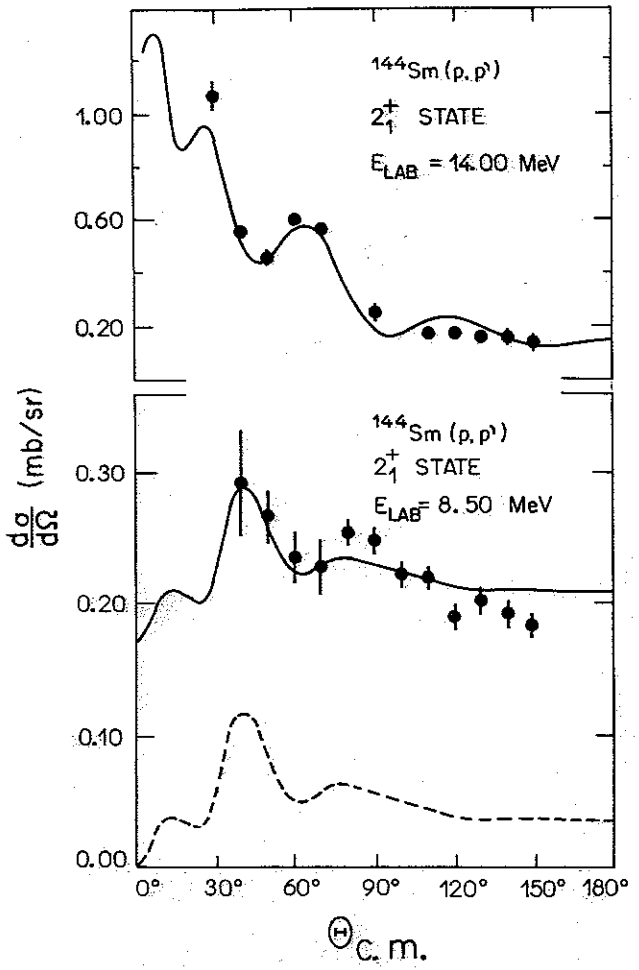
144Sm (p, p')
2+1 STATE
ELAB = 14.00 MeV
144Sm (p, p')
2+1 STATE
ELAB = 8.50 MeV
dσ/dΩ (mb/sr)
1.00
0.60
0.20
0.30
0.20
0.10
0.00
0°
30°
60°
90°
120°
150°
180°
Θ C. m.

FIG. 2

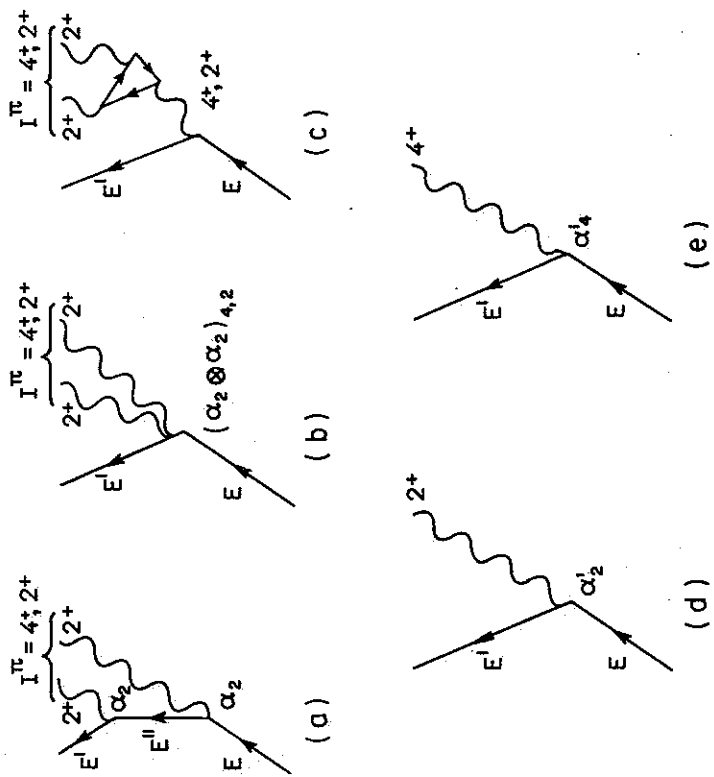
Iπ = 4+; 2+
2+
2+
4+; 2+
E'
E
(c)
Iπ = 4+; 2+
2+
2+
(α2 ⊗ α2)4,2
E'
E
(b)
Iπ = 4+; 2+
2+
2+
α2
α2
E'
E''
E
(a)
4+
α'4
E'
E
(e)
2+
α'2
E'
E
(d)

FIG. 3

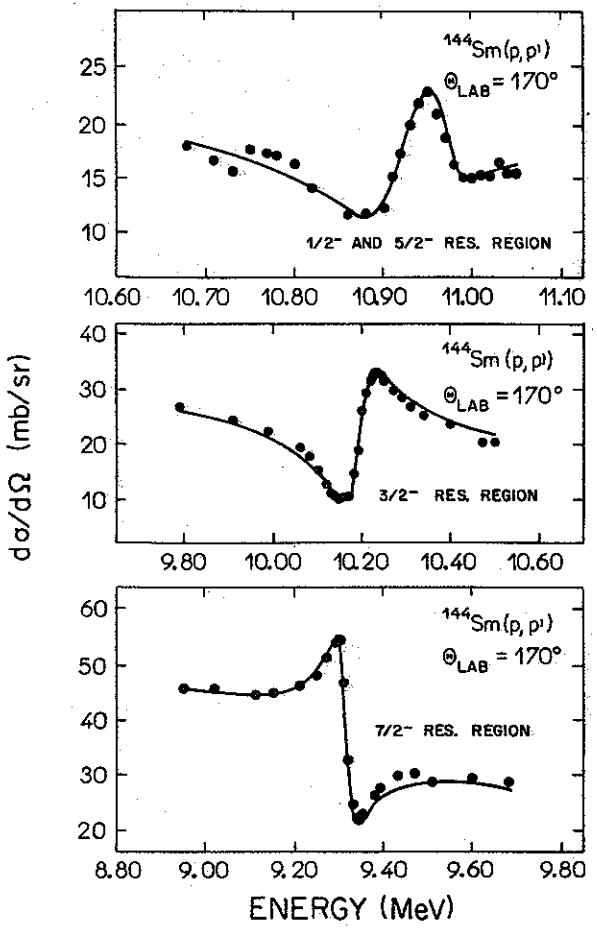
^{144}Sm(p,p$'$)
Θ_{LAB} = 170°
1/2⁻ AND 5/2⁻ RES. REGION
^{144}Sm (p, p$'$)
Θ_{LAB} = 170°
3/2⁻ RES. REGION
^{144}Sm(p, p$'$)
Θ_{LAB} = 170°
7/2⁻ RES. REGION
dσ/dΩ (mb/sr)
ENERGY (MeV)

FIG. 4

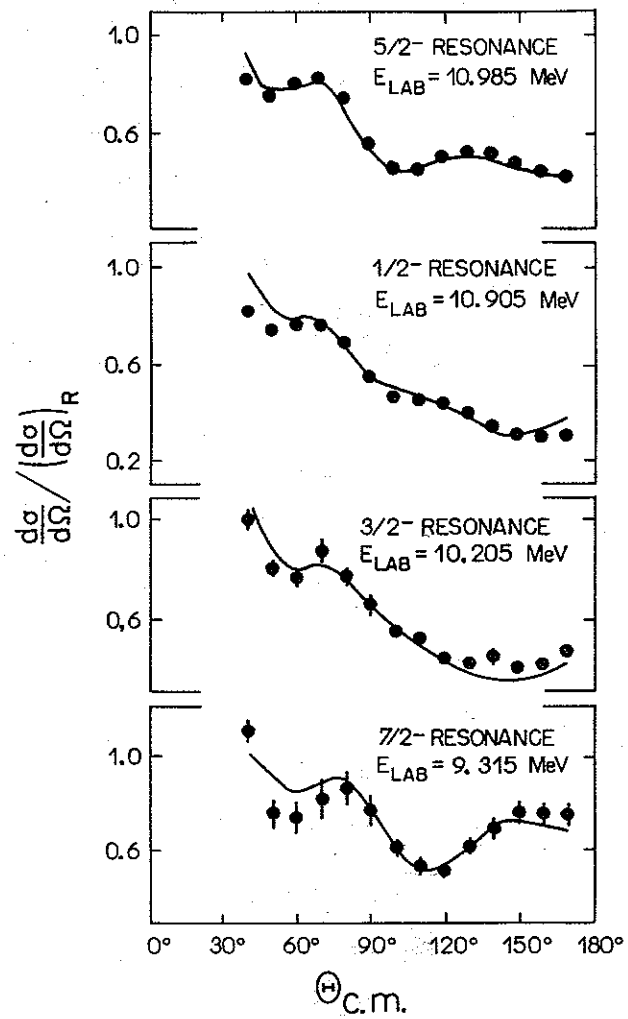
5/2⁻ RESONANCE
E_{LAB} = 10.985 MeV
1/2⁻ RESONANCE
E_{LAB} = 10.905 MeV
3/2⁻ RESONANCE
E_{LAB} = 10.205 MeV
7/2⁻ RESONANCE
E_{LAB} = 9.315 MeV
$\frac{d\sigma}{d\Omega} / \left(\frac{d\sigma}{d\Omega}\right)_R$
$\Theta_{C.M.}$

FIG. 5

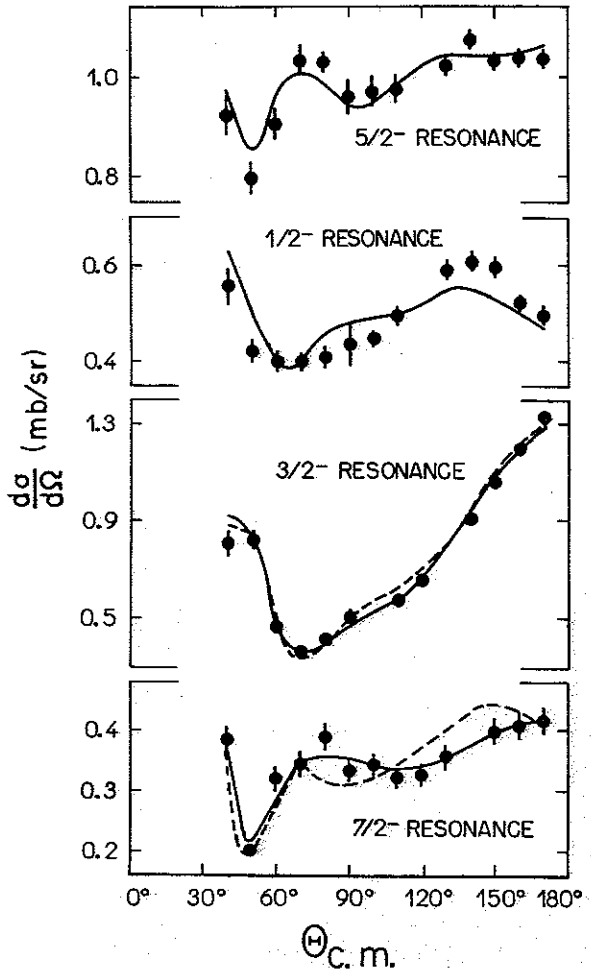
5/2⁻ RESONANCE
1/2⁻ RESONANCE
3/2⁻ RESONANCE
7/2⁻ RESONANCE
dσ/dΩ (mb/sr)
Θc.m.

FIG. 6

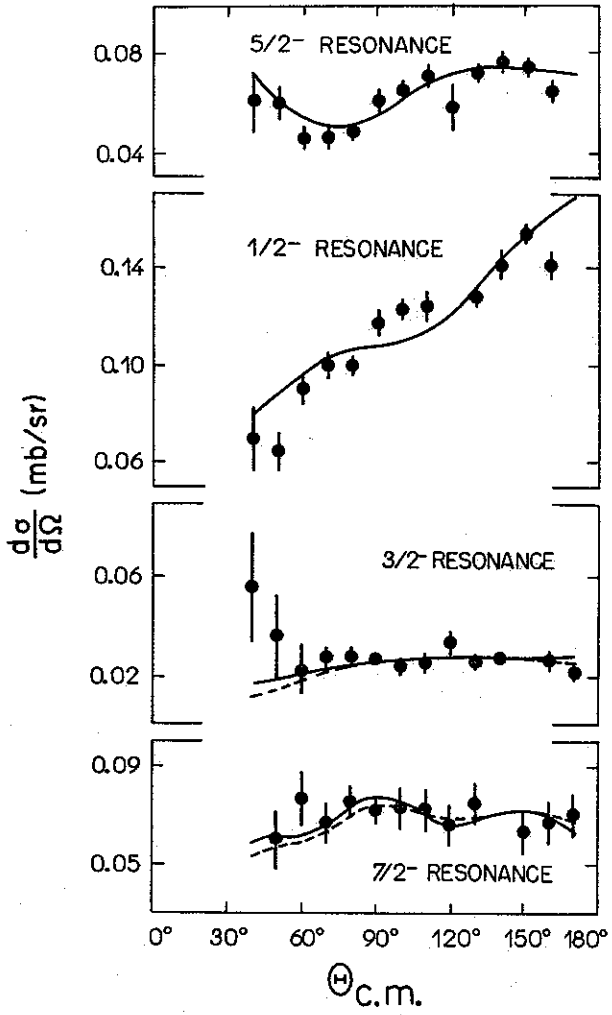
5/2⁻ RESONANCE
1/2⁻ RESONANCE
3/2⁻ RESONANCE
7/2⁻ RESONANCE
dσ/dΩ (mb/sr)
Θc.m.

FIG. 7

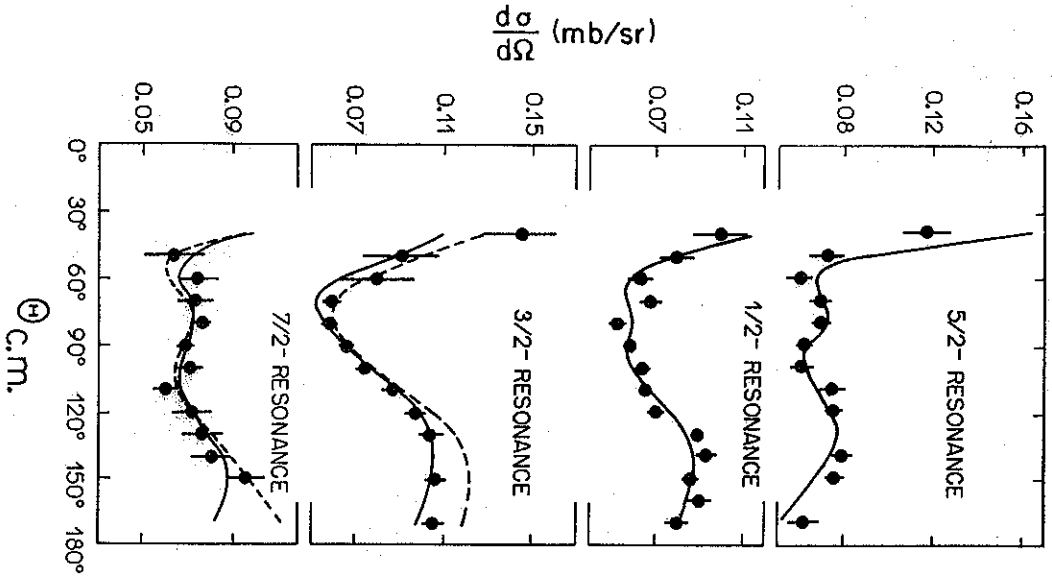
dσ/dΩ (mb/sr)
0.16
0.12
0.08
5/2- RESONANCE
0.11
0.07
1/2- RESONANCE
0.15
0.11
0.07
3/2- RESONANCE
0.09
0.05
7/2- RESONANCE
0°
30°
60°
90°
120°
150°
180°
Θ(H) C.m.

FIG. 8

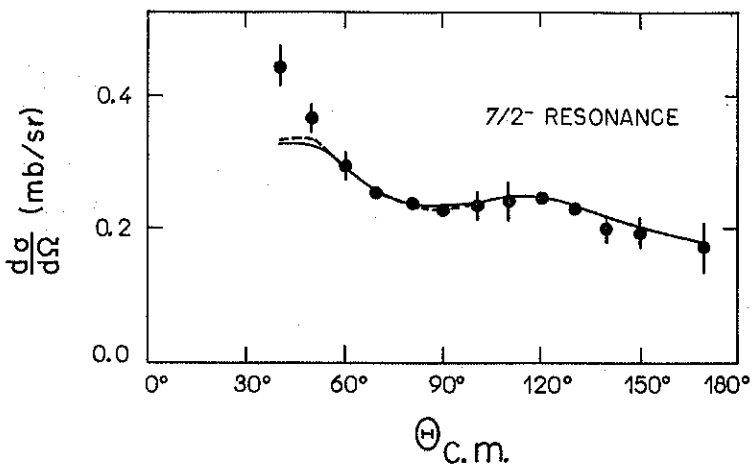
dσ/dΩ (mb/sr)
0.4
0.2
0.0
7/2- RESONANCE
0°
30°
60°
90°
120°
150°
180°
Θ(π) C.m.

FIG. 9

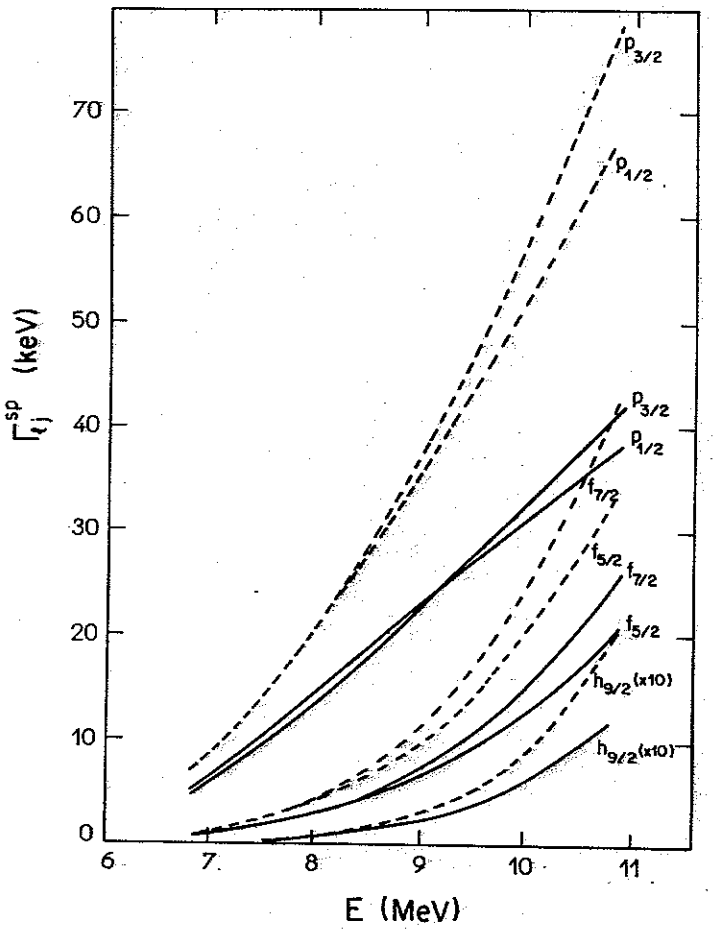
Γ^{sp}_{lj} (keV)
E (MeV)
$p_{3/2}$
$p_{1/2}$
$p_{3/2}$
$p_{1/2}$
$f_{7/2}$
$f_{5/2}$
$f_{7/2}$
$f_{5/2}$
$h_{9/2}$(x10)
$h_{9/2}$(x10)

FIG. 10

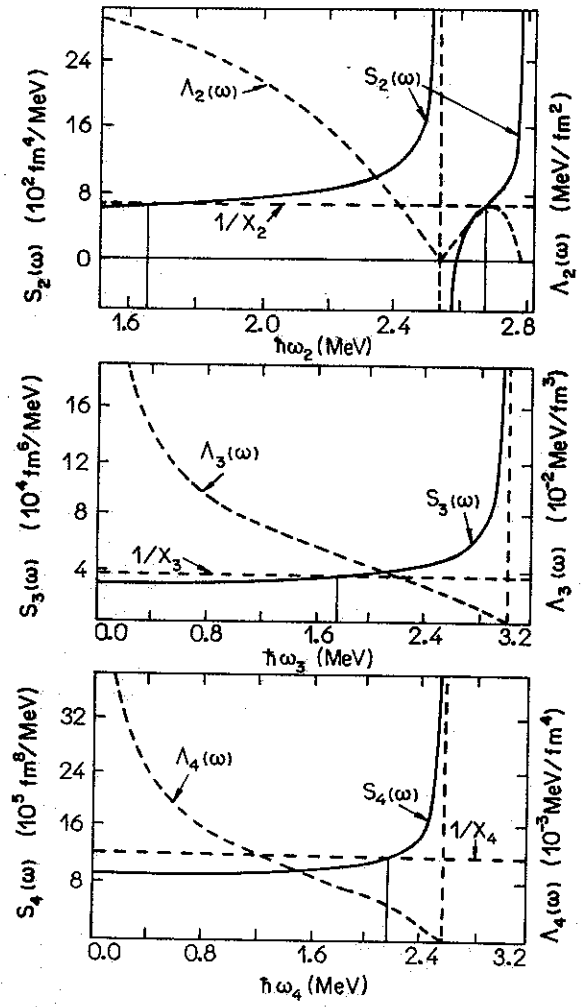
$\Lambda_2(\omega)$
$S_2(\omega)$
$1/X_2$
$S_2(\omega)$ (10^2 fm^4/MeV)
$\Lambda_2(\omega)$ (MeV/fm^2)
$\hbar\omega_2$ (MeV)
$\Lambda_3(\omega)$
$S_3(\omega)$
$1/X_3$
$S_3(\omega)$ (10^4 fm^6/MeV)
$\Lambda_3(\omega)$ (10^{-2} MeV/fm^3)
$\hbar\omega_3$ (MeV)
$\Lambda_4(\omega)$
$S_4(\omega)$
$1/X_4$
$S_4(\omega)$ (10^5 fm^8/MeV)
$\Lambda_4(\omega)$ (10^{-3} MeV/fm^4)
$\hbar\omega_4$ (MeV)

FIG. 11

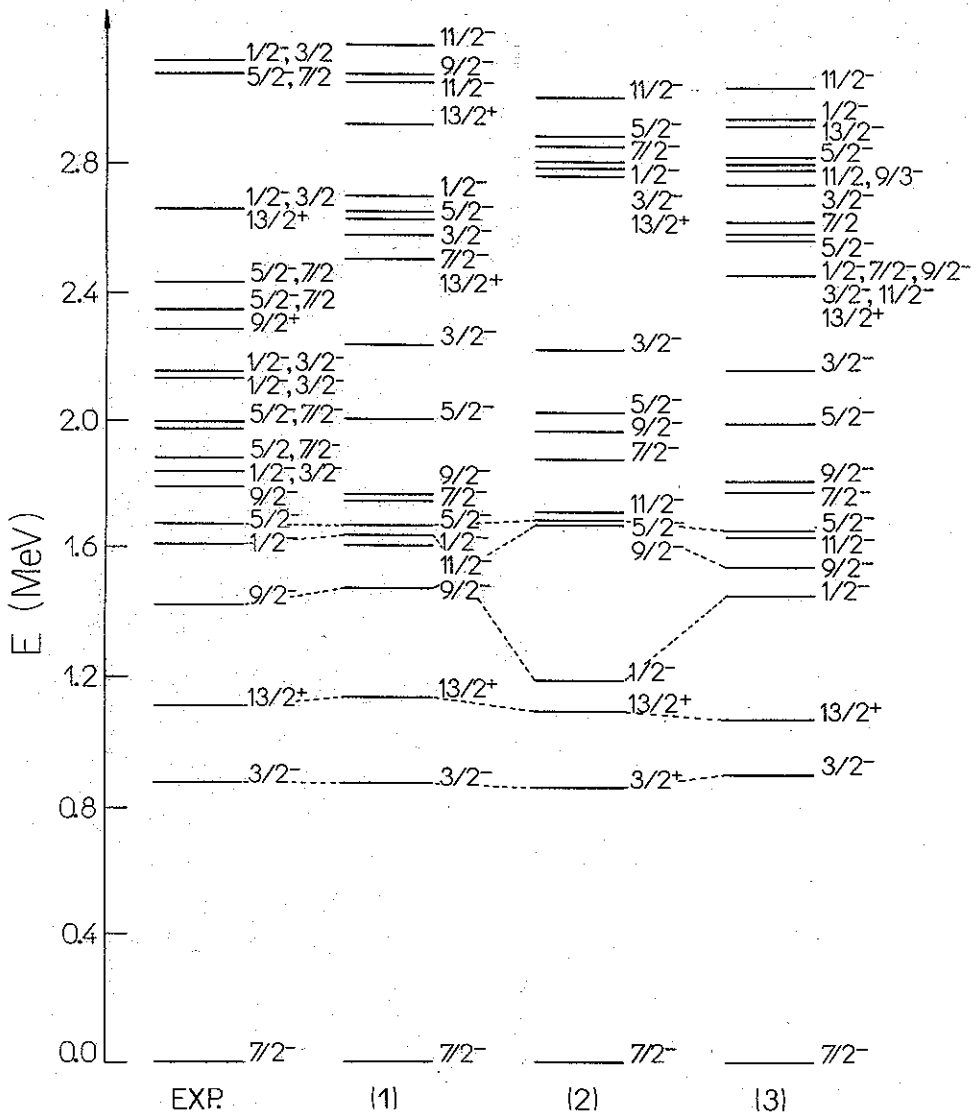
E (MeV)
0.0
0.4
0.8
1.2
1.6
2.0
2.4
2.8
EXP.
(1)
(2)
(3)
7/2⁻
1/2⁻, 3/2⁻
5/2⁻, 7/2⁻
13/2⁺
9/2⁺
5/2, 7/2⁻
1/2⁻
9/2⁻
5/2⁻
3/2⁻
11/2⁻
1/2⁻, 7/2⁻, 9/2⁻
3/2⁻, 11/2⁻
11/2, 9/3⁻

FIG. 12